THE ASTROPHYSICAL JOURNAL, 468:175–183, 1996 September 1

ASCA SPECTRA OF THE X-RAY FAINT S0 GALAXY NGC 4382

D.-W. KIM
Chungnam National University, Taejon 305–764, South Korea; and Harvard-Smithsonian Center for Astrophysics
G. FABBIANO
Harvard-Smithsonian Center for Astrophysics, 60 Garden Street, Cambridge, MA 02138
H. MATSUMOTO AND K. KOYAMA
Kyoto University, Kyoto 606-01, Japan
AND
G. TRINCHIERI
Osservatorio Astrofisico di Brera, Via Brera 28, Milano 20121, Italy; and Harvard-Smithsonian Center for Astrophysics
Received 1995 March 2; accepted 1996 March 14

ABSTRACT

NGC 4382 is one of the E and S0 galaxies detected with the lowest X-ray–to–optical luminosity ratio. These galaxies have a peculiar X-ray (0.1–3 keV) spectrum, with a significant excess of counts in the lowest spectral channels (<1 keV) relative to the spectral count distributions of X-ray brighter E and S0 galaxies. Analyzing the *ROSAT* Position Sensitive Proportional Counter observations of NGC 4382, it was unclear whether this soft excess were due to a real very soft component in a multicomponent spectrum or reflected an extremely low metal abundance in a isothermal hot gas. Our *ASCA* observations show that the low-abundance single-temperature model does not fit well the X-ray spectrum, in agreement with our previous suggestions. A better explanation is a composite spectrum with a very soft component (~0.3 keV) in addition to a hard, likely stellar, component (~5 keV). In this model, the abundance cannot be constrained. However, other more complex spectral models cannot be excluded.

Subject headings: galaxies: elliptical and lenticular, cD — galaxies: individual (NGC 4382) — X-rays: galaxies

1. INTRODUCTION

The S0 galaxy NGC 4382 is in the Virgo cluster, but it differs from other Virgo early-type galaxies by being rather inconspicuous in X-rays. Its X-ray–to–optical flux ratio is among the lowest detected in E and S0s and is a factor of ~100 smaller than those of X-ray bright Virgo and field galaxies of similar optical luminosity (Fig. 1). Although its X-ray detection was first attributed to a hot ISM, and used to estimate a binding mass (Forman, Jones, & Tucker 1985), it was soon realized that the X-ray emission may be dominated instead by a population of evolved stellar sources, similar to those present in the bulge of M31 (Trinchieri, Fabbiano, & Canizares 1986; Canizares, Fabbiano, & Trinchieri 1987). These sources have an X-ray spectrum typically harder than that of the hot interstellar matter (ISM) of X-ray bright E and S0s (Fabbiano, Trinchieri, & Van Speybroeck 1987; Kim, Fabbiano, & Trinchieri 1992a). Spectral observations could therefore establish the nature of the X-ray emission of NGC 4382 and of other similarly X-ray faint E and S0s.

The results of spectral analyses based on *Einstein* and *ROSAT* data present however, a puzzling picture. Although NGC 4382 was too faint to warrant individual analysis of its *Einstein* IPC data, it belongs to the sample of E and S0s selected on the basis of their small X-ray–to–optical ratio, which have a peculiar soft excess in their average *Einstein* spectral count distribution (Kim et al. 1992b). This spectrum is very different both from the ~1 keV thermal spectrum of X-ray bright E and S0 galaxies and from the harder spectrum expected from a collection of low-mass binaries. Subsequent *ROSAT* Position Sensitive Proportional Counter (PSPC) observations (Fabbiano, Kim, & Trinchieri 1994) confirmed the *Einstein* results, revealing a PSPC spectral count distribution in NGC 4382 significantly different from those of X-ray bright galaxies, with a relative excess of counts in the lower energy spectral channels.

However, the limited resolution and bandwidth of the PSPC do not allow us to distinguish between different sets of emission models. The PSPC data can be equally well fitted with a very low metallicity plasma of $kT \sim 0.6$ keV, a bremsstrahlung emission of the same kT, or a two-component model consisting of a solar abundance plasma with $kT \sim 0.2$ keV plus a harder (>1 keV) component contributing similar amounts of the emission (Fabbiano et al. 1994). More complicated models, however, cannot be excluded (e.g., Pellegrini & Fabbiano 1994). Two- or multicomponent models are more appealing in terms of physically plausibility (Fabbiano et al. 1994), since they do not require assumptions about either a new population of X-ray sources or the presence of a metal-free (therefore primordial) plasma.

In order to establish the nature of the X-ray emission of this X-ray faint early-type galaxy, we observed NGC 4382 with *ASCA* (Tanaka, Inoue, & Holt 1994). These higher spectral resolution data make the low-abundance single-temperature model very unlikely and confirm the existence of a complex emission spectrum, including a very soft component.

In § 2 we describe the *ASCA* observations and data reduction (§ 2.1), and we present spectral analysis (§ 2.2) and results (§ 2.3). In § 3 we discuss the nature of the very soft component and the implications of our results.

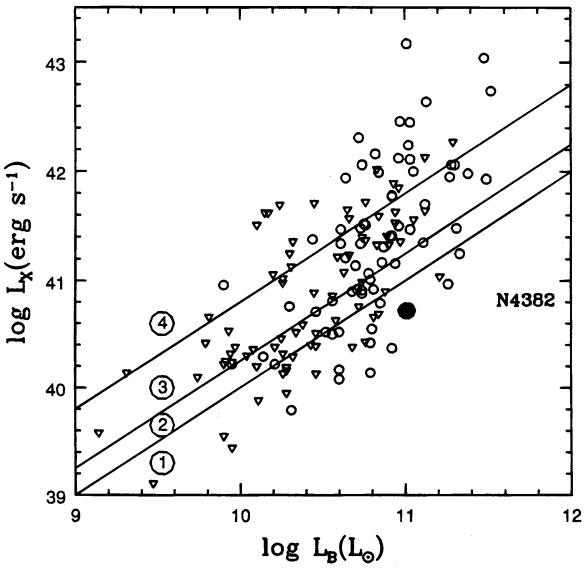

FIG. 1.—L_X-L_B diagram of E and S0 galaxies. All data are from Fabbiano et al. (1992). The diagonal lines delimit the four spectral groups (1–4) of Kim et al. (1992b). Group 3 and 4 galaxies have ~1 keV average spectra in *Einstein*. Group 2 galaxies have hard spectra (>2 keV), and Group 1 galaxies have a spectrum that can be fitted with a mixture of a hard and a very soft (~0.2 keV) component. The locus of spiral galaxies and spiral bulges (dominated by discrete binary sources) in this plot corresponds with the group 1 and 2 regions. The circle and triangle indicate detections and upper limits.

2. X-RAY OBSERVATIONS AND DATA ANALYSIS

2.1. *Data Screening and Background Determination*

NGC 4382 was observed on 1994 May 27–28 with *ASCA* using both solid-state imaging spectrometer (SIS) (Burke et al. 1991) and the gas imaging spectrometer (GIS) (Ohashi et al. 1991). The observational log and basic parameters of the galaxy are given in Table 1. The data were screened using the screening package XSELECT/ASCASCREEN with the default selection criteria. This method excludes data affected by the South Atlantic Anomaly, Earth occultation, and regions of low geomagnetic rigidity. We also eliminated contamination by the bright Earth, removed hot and flickering pixels for the SIS data, and applied rise time rejection to exclude particle events for the GIS data (Day et al. 1994). This screening was applied separately to data collected in each instrument mode, i.e., to six data sets (two GIS detectors; 1- and 2-CCD modes for two SIS detectors).

TABLE 1

BASIC PARAMETERS

Parameter	Value
R.A. (J2000)[a,b]	12 25 24.7
Decl. (J2000)[a,b]	18 11 27
B_T^0 (mag)[b]	9.99
D (Mpc)[c]	27.0
D_{25} (arcsec)[b]	425
N_H (cm^{-2})[d]	2.7×10^{20}
ASCA observed date	1994 May 27–28
ASCA net good time (s)	32,000–35,000[e]
Log F_X (IPC) (ergs s^{-1} cm^{-2})[f]	$(6.0 \pm 0.5) \times 10^{-13}$
Log F_X (PSPC) (ergs s^{-1} cm^{-2})[g]	$(7.3 \pm 0.5) \times 10^{-13}$

[a] Units of right ascension are hours, minutes, and seconds, and units of declination are degrees, arcminutes, and arcseconds.

[b] Right ascension (R.A.), declination (decl.), total face-on B magnitude (B_T^0), and major isophotal diameter measured at $B = 25$ mag arcsec^{-2} (D_{25}) taken from de Vaucouleurs et al. 1991.

[c] Distance from Fabbiano et al. 1992.

[d] Galactic line-of-sight H column density from Stark et al. 1992.

[e] The net good times are 32.9 ks for SIS0, 32.2 ks for SIS1, and 35.0 ks for GIS2 and GIS3.

[f] IPC flux from Fabbiano et al. 1992. Fluxes were estimated in an energy range of 0.2–4.0 keV and $kT = 1$ keV was assumed. The count extraction radius is $r = 240''$, and the error is a statistical one.

[g] PSPC flux from Fabbiano et al. 1994. Fluxes were estimated in an energy range of 0.1–2.0 keV and a two-component model was used. The count extraction radius is $r = 220''$, and the error is a statistical one.

In Figure 2 images from the SIS 2-CCD mode and GIS3 are shown; in Figure 3 the *ROSAT* PSPC image is shown for comparison. A strong source coincides with the optical position of NGC 4382. The *ROSAT* PSPC observation revealed several serendipitous sources within ~15′ of NGC 4382 (Fabbiano et al. 1994). Sources are seen in the SIS and GIS images at 2.′8 Northwest, 7.′0 North, 13.′7 Northwest, and 15.′9 South (GIS only) from the center of NGC 4382. However, because of the poor point response function of the *ASCA* detectors, the corresponding source shapes are much broader and more asymmetrical than in the PSPC. Furthermore, the surface brightness distribution appears different in the different detectors, because of the misalignment of the four telescopes associated with the detectors.

To generate spectra for further analysis, SIS data in the 1- and 2-CCD modes were combined because the telescope pointings were the same for these two modes. This resulted in four data sets.

We used three different approaches for subtracting the field background contribution from the source counts: (1) we derived the background locally in a source-free region in the same chip for the SIS data, and at a similar off-center distance for the GIS; (2) for the SIS 2-CCD observations only, we derived the background from the second (source free) chip; and (3) we used the "deep blank sky data" (several performance verification [PV] phase observations combined) provided by the *ASCA* Guest Observer Facility (GOF). There are some disadvantages to all methods. In the first two methods, the background and source regions have different detector responses and the current available spectral package (XSPEC) ignores this difference. In the third method, although the source and background regions are the same, the deep sky data do not correctly reflect temporal and spatial variations of the background of the observed field. Nevertheless, the three estimates of the background produce consistent results in our spectral fitting analysis, and therefore these potential problems do not affect our results. In the following, we will report the results obtained with local background subtraction.

2.2. *Spectral Analysis*

The source spectrum was extracted from circles of radius 3′ and 5′ for the SIS and GIS data, respectively. In both cases the circle was centered on the emission peak. These count extraction radii were determined by examining the radial profile of X-ray surface brightness in each detector. The extraction parameters are given in Table 2. We used XSPEC for the spectral analysis. For *ASCA* response files, the redistribution matrix (RMF) v0.6 for SIS and v3.1 for GIS were obtained from the *ASCA* GOF, and the position-dependent effective area curve (ARF) for each detector was generated at the source position. We have also tried a new version v0.8 for SIS and v4.0 for GIS, but no difference was found in our results. Prior to model fitting, we rebinned the

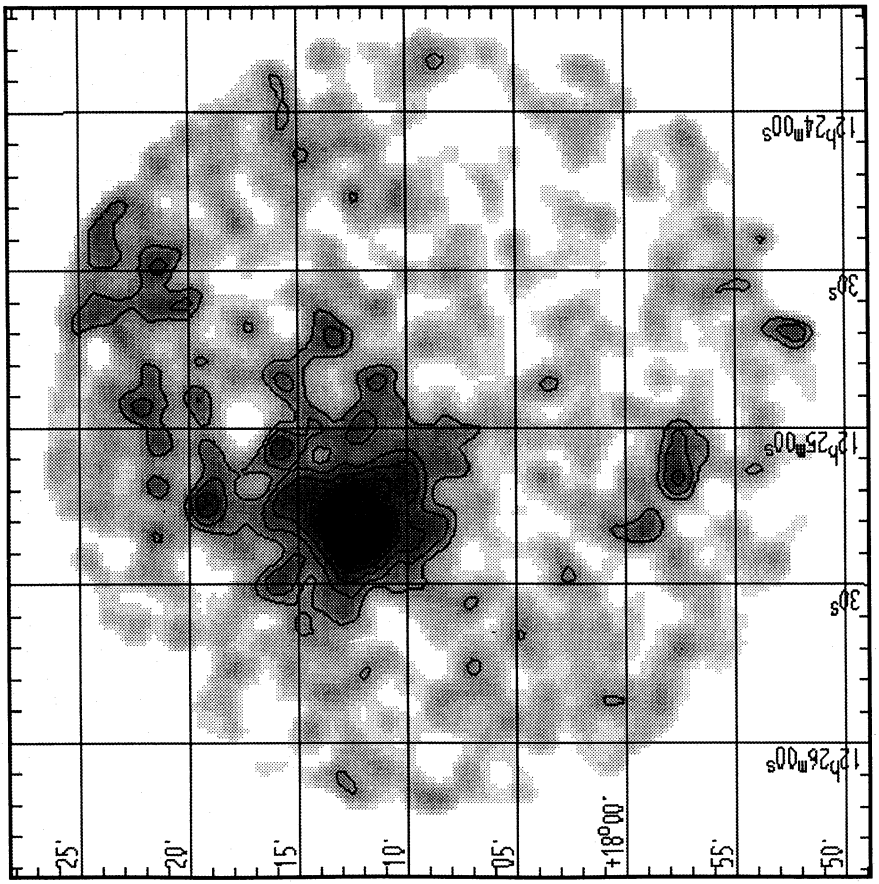

FIG. 2b

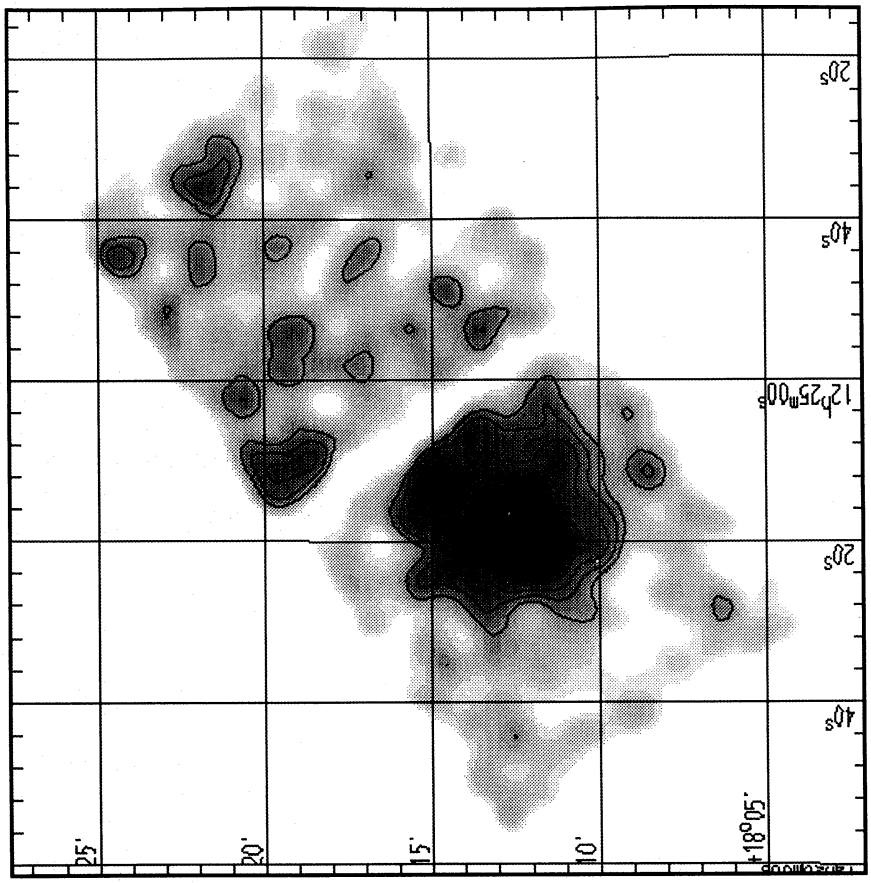

FIG. 2a

FIG. 2.—*ASCA* X-ray images. The images were taken (*a*) in a SIS1 2-CCD mode and (*b*) with GIS3. Both images were smoothed with a Gaussian of $\sigma = 30''$.

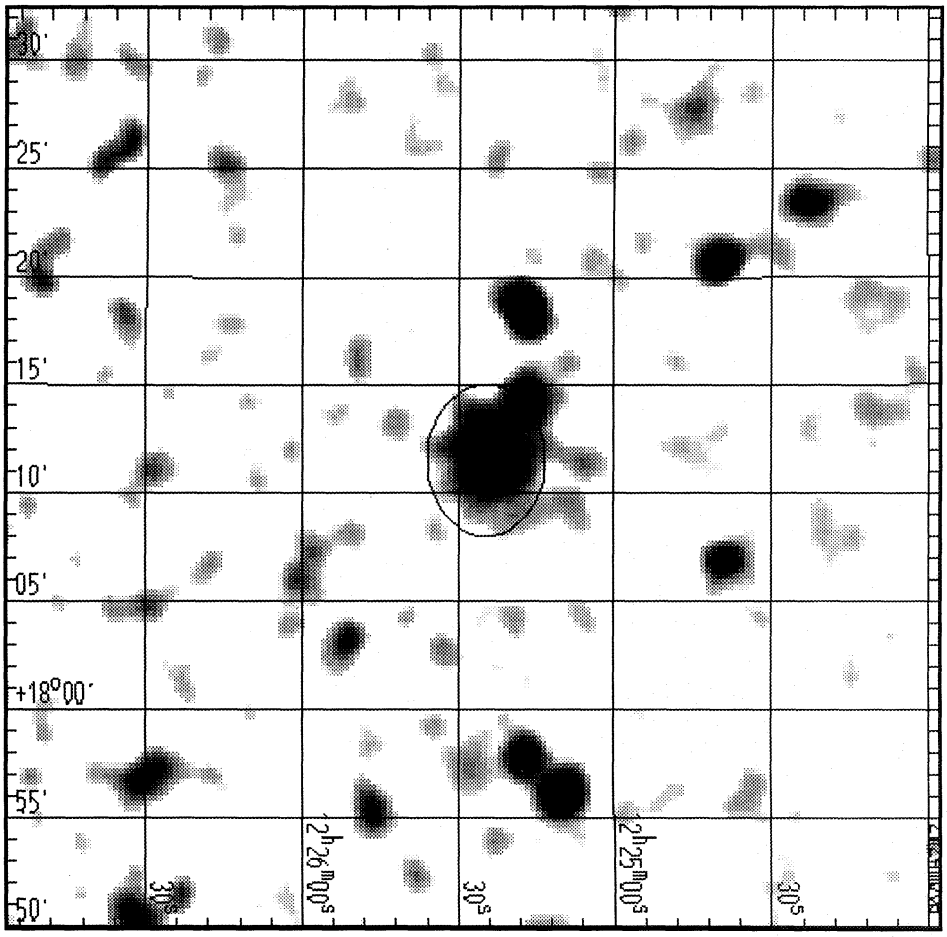

FIG. 3.—*ROSAT* PSPC image of NGC 4382. The ellipse indicates the optical galaxy at $B = 25$ mag isophote. The image was smoothed with a Gaussian of $\sigma = 30''$.

data so that each spectral bin contains at least 20 counts.

In Table 2 we also list counts and count rates for each detector. The count rates are different for each detector, because of different detector responses. Spectral fitting done with the same source normalization (i.e., emission measure) are consistent with all the data except for that from GIS3. Counts in the GIS3 spectrum are larger than expected with its detector response, most likely a consequence of incomplete detector calibration. An emission measure increase by a factor of 1.3 would be required to reproduce the GIS3 spectrum. However, this inconsistency does not affect the spectral fitting results, because the SIS spectra mainly control the spectral fitting; therefore, we use the same emission measure for simultaneous fits of SIS and GIS spectra. We also fitted the SIS and GIS spectra separately. The results are similar except for the normalizations.

We tested the effect of using slightly different source radii (e.g., 4′ for SIS and/or GIS) on the spectral results, performing the same analysis. The results do not differ appreciably. We also repeated the analysis by explicitly including and excluding the source at 2.′8 northwest from the center of NGC 4382. Again, we obtain consistent results.

2.3. *Results*

The results of the spectral analysis are summarized in Table 3 and Figures 4–6. A single-temperature Raymond model (a revised version of Raymond & Smith 1977) with fixed solar abundance gives a very poor fit to the data. Not

TABLE 2

COUNTS

	X (det)[a]	Y (det)[a]	r (arcsec)	Exposure (s)	Counts	Background	Net	Rate (counts ks^{-1})
SIS0	113	111	180	32,903.26	1178	405	773	23.49 ± 1.18
SIS1	111	118	180	32,158.98	967	436	531	16.51 ± 1.13
GIS2.....	106	115	300	34,983.24	876	421	455	13.01 ± 0.93
GIS3.....	109	113	300	34,927.24	1073	420	653	18.70 ± 1.02

NOTE.—Background region (in detector coordinates): SIS0 BOX (102.50, 68.50, 79.00, 21.00) + BOX(71, 104, 79.00, 22.00, 90.000); SIS1 BOX(102.50, 68.50, 79.00, 21.00) + BOX(71.104, 79.00, 22.00, 90.000); GIS2 CIRCLE(160, 139, 30); GIS3 CIRCLE(157, 140, 30).

[a] Unbinned detector coordinates for GIS and binned (by factor of 4) detector coordinates for SIS.

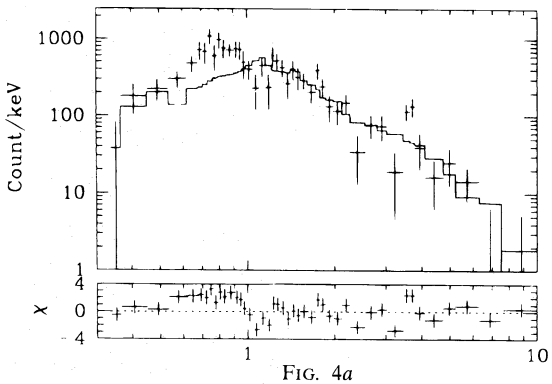

FIG. 4a

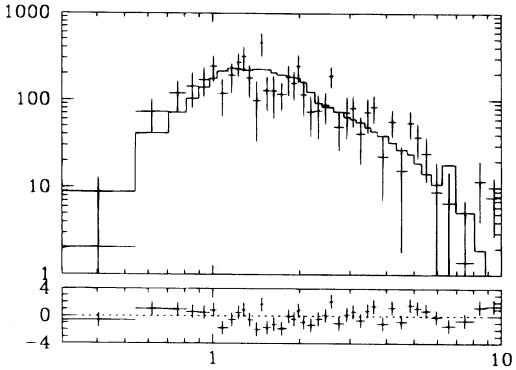

FIG. 4b

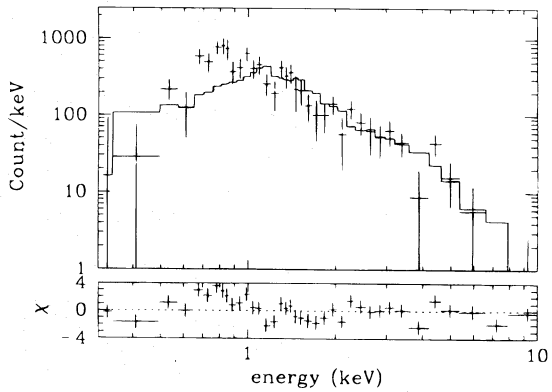

FIG. 4c

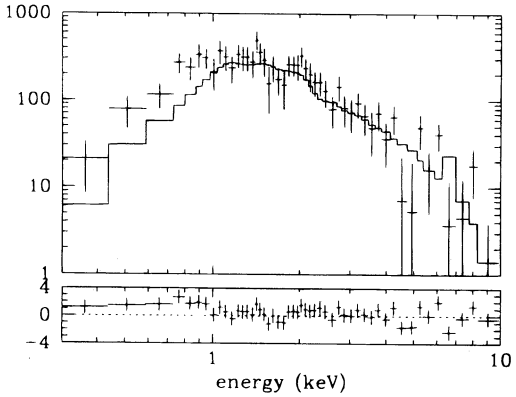

FIG. 4d

FIG. 4.—Joint fit of two SIS and two GIS spectra. (*a*) SIS0; (*b*) SIS1; (*c*) GIS2; and (*d*) GIS3. The solid histogram indicates the best-fit one-component Raymond thermal model with a fixed solar abundance. The bottom panel shows δ_χ = (observed − predicted)/(observed error).

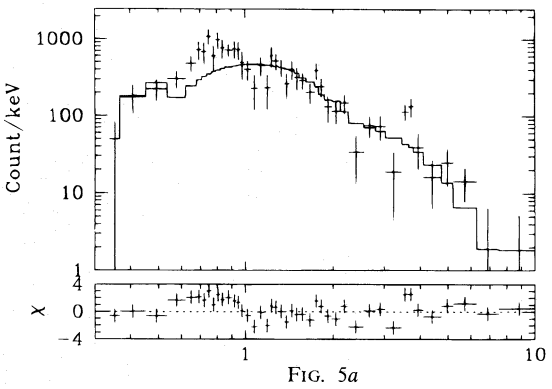

FIG. 5a

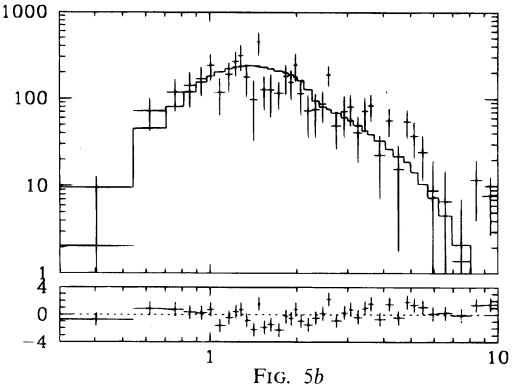

FIG. 5b

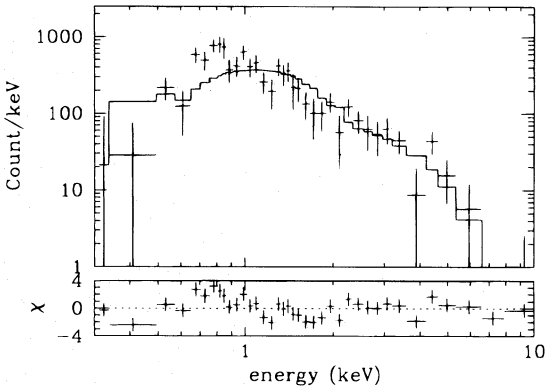

FIG. 5c

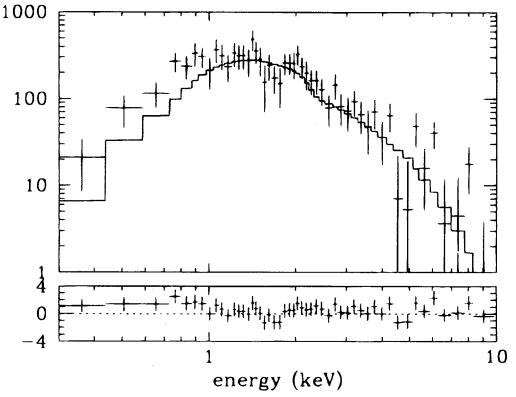

FIG. 5d

FIG. 5.—Same as Fig. 4 except for varying the abundance

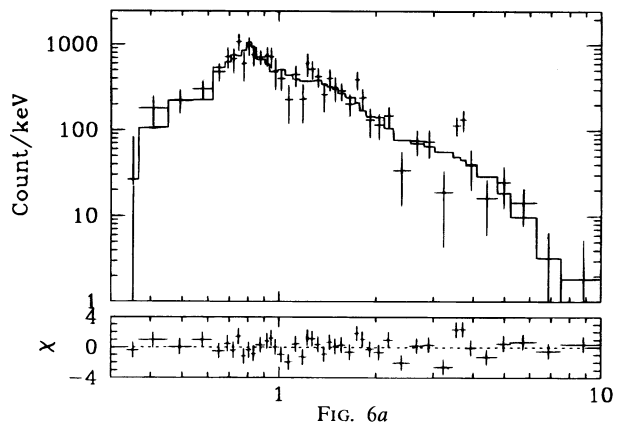

FIG. 6a

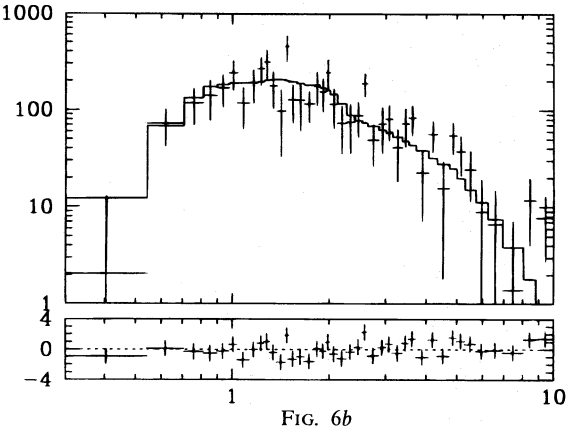

FIG. 6b

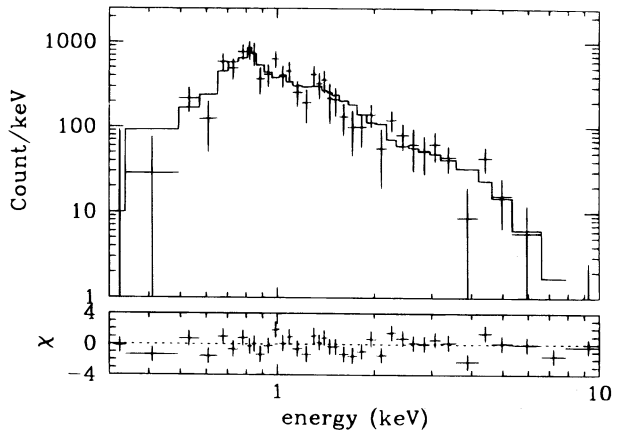

FIG. 6c

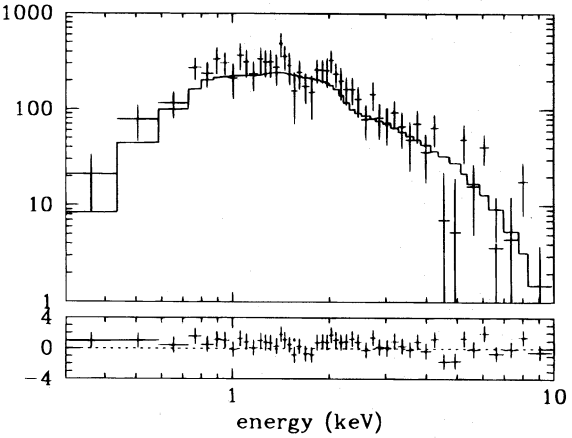

FIG. 6d

FIG. 6.—Same as Fig. 4 except for a two-component model

TABLE 3

SPECTRAL FIT

A. SINGLE-TEMPERATURE MODEL WITH SOLAR ABUNDANCE[a]

Spectra	N_H (10^{20} cm^{-2})	kT (keV)	χ^2	Degrees of Freedom
SIS	0	5.1	197	79
GIS	0	4.2	113	88
SIS+GIS	0	4.7	310	170
SIS+GIS+PSPC	0.26	4.6	356	192

B. SINGLE-TEMPERATURE MODEL WITH VARYING ABUNDANCE

Spectra	N_H (10^{20} cm^{-2})	kT (keV)	Z (solar)	χ^2	Degrees of Freedom
SIS	0	2.5	0	161	78
GIS	0	4.4	0.03	107	87
SIS+GIS	0	3.3	0	274	169
SIS+GIS+PSPC	0.73	3.1	0	311	191

C. RAYMOND + BREMSSTRAHLUNG MODEL WITH SOLAR ABUNDANCE[a]

Spectra	N_H[b] (10^{20} cm^{-2})	kT_1[b] (keV)	kT_2[b] (keV)	χ^2	Degrees of Freedom
SIS	6.7 (<27.2)	0.30 (0.23–0.42)	4.9 (2.6–13.2)	88	77
GIS	11 (<123)	0.30 (0.11–0.82)	6.1 (2.5–16.5)	87	86
SIS+GIS	6.9 (<25.8)	0.31 (0.24–0.43)	5.6 (3.6–10.4)	179	168
SIS+GIS+PSPC[c]	0.80 (0.26–1.61)	0.33 (0.27–0.41)	6.4 (4.3–12.8)	196	190

[a] The solar abundance is from Anders & Grevesse 1989, i.e., [Fe]/[H] = 4.68×10^{-5}.
[b] The acceptable range is in 90% confidence for three interesting parameters.
[c] Varying the abundance, we obtain the best-fit $Z = 2.45$ (>10%) solar at 90% confidence.

only is χ^2 too large, but there is also excess emission over the best-fit model in the 0.5–1 keV energy range. This excess clearly indicates the presence of a secondary emission component. Allowing the metal abundance to vary freely, we obtained a somewhat lower minimum χ^2. However, the reduction is not substantial, and moreover the excess in 0.5–1 keV still exists (see Figure 5). In this case the best-fit abundance is almost zero, i.e., the model is close to pure bremsstrahlung with no line emission.

Instead, a two-component model, consisting of a low-temperature Raymond thermal model with solar abundance plus a higher temperature bremsstrahlung model, fits the data well, without any significant residuals at any energies (see Fig. 6). The significance of the secondary component determined by the F test is more than 99.9%. The best-fit kT parameters are 0.3 keV for the soft thermal emission and $\sim$6 keV for the bremsstrahlung emission. The confidence ranges of the two temperatures are well determined (Table 3 and Fig. 7). In particular, the temperature of the soft component is well constrained in a narrow range 0.24–0.43 keV at 90% confidence for three interesting parameters (Avni 1976). The temperature of the hard component is constrained by the joint SIS-GIS fit to be between 3.6 and 10.4 keV. The acceptable ranges of the abundance and absorption column density are not well determined. If we use a Raymond model instead of a bremsstrahlung model for the hard component, the result is almost the same, because emission lines are not significant at this high temperature in the detected energy range.

We have also used the *ROSAT* PSPC spectra taken from Fabbiano et al. (1994) and jointly fit the *ASCA* and PSPC spectra. The PSPC instrument has a larger effective area at the low energies, therefore the joint *ASCA*+PSPC fit can provide narrower constraints on the absorption column density and soft component. The results are listed in Table 3. While the best-fit temperatures of the two components are almost the same, the absorption column density is lower and well constrained.

If we let the abundance vary, the best-fit abundance is 2.5 times solar, although its error range is undetermined (>10% solar at 90% confidence).

In Table 4 we list fluxes and luminosities of each emission component and the total emission. These are absorption-corrected intrinsic quantities and determined with the spectral parameters of the joint *ASCA*+PSPC fit. The soft component contributes $\sim$40% of the flux in the 0.1–2.0 keV range, consistent with the *ROSAT* results for the same spectral model, but it contributes only $\sim$20% of the total emis-

TABLE 4

FLUX AND LUMINOSITY[a]

Parameter	Soft Component	Hard Component	Total Emission
F_X (0.1–2 keV)	2.5 + 0.5	3.8 ± 0.7	6.3 ± 1.3
F_X (0.2–4 keV)	2.2 ± 0.5	5.5 ± 1.1	7.8 ± 1.6
F_X (0.25–10 keV).....	2.2 ± 0.5	8.0 ± 1.5	10.1 ± 2.0
L_X (0.1–2 keV)	2.1 ± 0.5	3.3 ± 0.6	5.5 ± 1.1
L_X (0.2–4 keV)	2.0 ± 0.4	4.8 ± 0.9	6.8 ± 1.4
L_X (0.25–10 keV).....	1.9 ± 0.4	7.0 ± 1.3	8.8 ± 1.8

[a] The flux is in unit of 10^{-13} ergs s^{-1} cm^{-2}, and luminosity is in units of 10^{40} ergs s^{-1}. The flux and luminosity are absorption-corrected intrinsic quantities. Distance = 27 Mpc. The error (1 σ) is calculated by estimating the acceptable range of normalization. The statistical error is negligible.

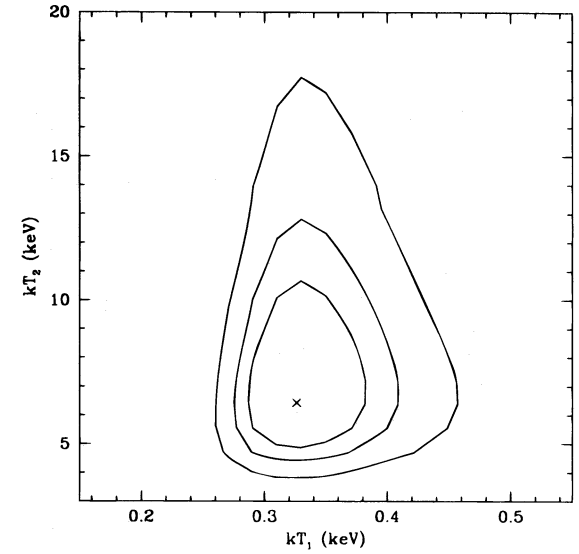

FIG. 7*a*

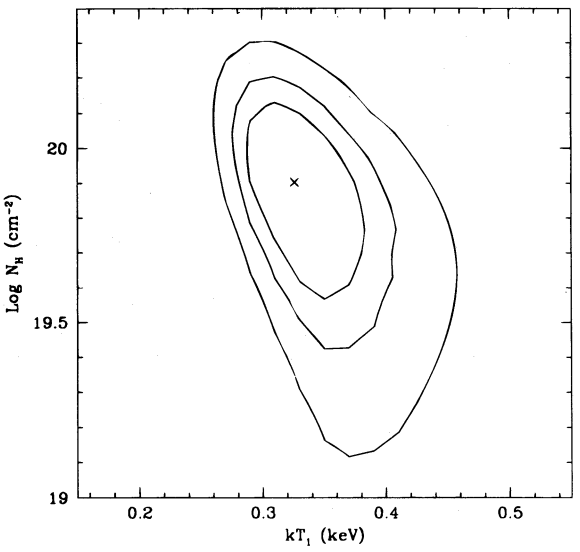

FIG. 7*b*

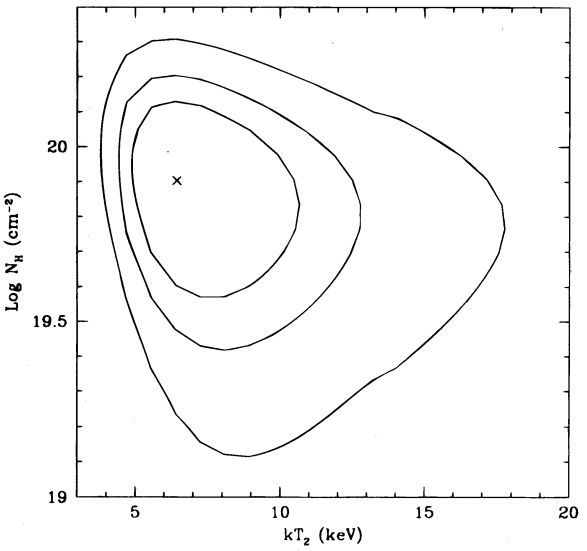

FIG. 7*c*

FIG. 7.—χ^2 contour plots for (*a*) kT_1 and kT_2, (*b*) kT_1 and N_H, and (*c*) kT_2 and N_H. The three contours are 68%, 90%, and 99% confidence levels with three interesting parameters for a joint *ASCA* + PSPC fit.

sion in the 0.25–10 keV range. The total flux is 1.0×10^{-12} ergs cm^{-2} s^{-1} in the 0.25–10 keV range.

The best-fit value of the absorption column density is 0.8×10^{20}. The allowed range at 90% confidence is $(0.3–1.6) \times 10^{20}$ (Table 3). The line-of-sight value, 2.7×10^{20} (Table 1), is excluded at 99% confidence. This occurs only when we fit the PSPC and *ASCA* spectra simultaneously. There may be some relative calibration problem between the PSPC and *ASCA*. We have tried with different normalizations for the two data sets, but the discrepancy still remains. If the fact that N_H is lower than the galactic line-of-sight value is really significant, then a more complicated model is required, e.g., adding another soft component. By adding a 0.1 keV component, the allowed N_H range is $(0.2–4) \times 10^{20}$. For lower values of N_H, the additional component contributes negligibly to the total emission (i.e., the same as Table 3). For higher values of N_H, the additional component increases to compensate for the larger absorption. This may suggest multitemperature soft emission. However, this may be overinterpretation of the current data.

We considered the uncertainties in calibration and plasma emission codes to better understand the robustness of our results. The *ASCA* instruments are known to have some calibration problems. In particular, *ASCA* spectra of several galaxy clusters indicate a large amount of excess absorption, which is inconsistent with previous observations (L. David and A. Prestwich 1994, private communication: see also ASCANEWS communication of 1995 December 11). However, this calibration error will not remove the need for a very soft component, because our spectra have excess soft counts, not the deficit expected at the soft energies because of this calibration problem. Another known problem is that currently available plasma emission codes produce too much emission at the Fe *L* line 4–2 transitions at $\sim$1.5 keV (N. Brickhouse 1994, private communication; Fabian et al. 1994). Again, this $\sim$1.5 keV line emission will not significantly affect the existence of a very soft component. Even in an extreme case where all the emission lines are uncertain, the spectral fit with a single-component model with almost zero abundance (therefore no lines) is still not acceptable.

3. DISCUSSION

Our *ASCA* observations of NGC 4382 help us constrain models of the X-ray emission of this galaxy and by inference of low-X-ray luminosity early-type galaxies. The results of the spectral fit exclude a single-temperature low-metallicity model and point to a multicomponent emission, consisting of at least two components: a hard component ($kT \sim$ 4–13 keV), and a very soft component ($kT \sim$ 0.2–0.4 keV). The two components contribute to the flux in similar amounts in the 0.1–2 keV band, consistent with the *ROSAT* results (Fabbiano et al. 1994), but in a wider energy band (0.25–10 keV), the soft component amounts to only one-fourth of the total emission. An even softer component ($\lesssim$0.1 keV) may be present, but the present data and SIS soft-band calibration make this possibility rather uncertain.

The existence of a hard component in the emission of E and S0 galaxies, due to the integrated emission of low-mass X-ray binaries, had been postulated early on (Trinchieri & Fabbiano 1985). This component was suggested by comparisons of the L_X–L_B dependence of E and S0s with that of spirals (Trinchieri & Fabbiano 1985; Canizares et al. 1987; Fabbiano, Gioia, & Trinchieri 1989; Eskridge, Fabbiano, & Kim 1995) and was first glimpsed in the co-added *Einstein* IPC spectra of X-ray faint E and S0s (Kim et al. 1992a, 1992b). This component has now been detected with *ASCA* in virtually all early-type galaxies (Matsushita et al. 1994), and its luminosity scales approximately linearly with the optical luminosity (T. Ohashi 1994, private communication), pointing to a stellar origin, as seen in spiral galaxies (Fabbiano & Trinchieri 1985; Fabbiano et al. 1989). The X-ray–to–optical ratio of this component is consistent with that of spiral galaxies and in particular with bulge-dominated spirals, where the X-ray emission is likely to be dominated by a population of low-mass binaries (e.g., M31; Trinchieri & Fabbiano 1991).

The existence of a very soft emission spectrum in X-ray faint E and S0 galaxies was first seen with the *Einstein* IPC (Kim et al. 1992b) and later confirmed with the *ROSAT* PSPC (Fabbiano et al. 1994; Fabbiano & Schweizer 1995). *ASCA* confirms that this emission is truly due to a very soft emission component in a multi-component spectrum. The very soft component, characterized by $\sim$0.3 keV thermal emission, emits 2×10^{40} ergs sec^{-1} in the range 0.25–10 keV (see Table 4).

Kim et al. (1992b), Fabbiano et al. (1994), and Pellegrini & Fabbiano (1994) considered possible candidates for the very soft component. It is possible that X-ray faint E and S0 do not retain a hot ISM. In this case, candidates include stellar sources, such as M star coronae (Schmitt et al. 1990), RS CVn (Dempsey et al. 1993), and supersoft sources such as those discovered with *ROSAT* in nearby galaxies (e.g., Greiner, Hasinger, & Kahabka 1991; Kahabka, Pietsch, & Hasinger 1994). If the very soft component is totally or in part related to stellar sources, it should exist in all early-type galaxies, although its contribution may be relatively small in X-ray bright early-type galaxies where strong, hot gaseous emission ($\sim$1 keV) dominates. However, hydrodynamic simulations (Pellegrini & Fabbiano 1994) suggest that the X-ray emission of X-ray faint E and S0 galaxies may be more complex than the simple two-temperature model we have here fitted to the data. X-ray faint early-type galaxies may contain a hot ISM that is cooler than that present in X-ray bright E and S0s, depending on the potential and supernova Ia rate of the galaxy. In particular, Pellegrini & Fabbiano (1994) showed that the *ROSAT* PSPC spectrum of the X-ray faint E galaxy NGC 4365 could be modeled with a three-component model including very soft and hard stellar components, plus a hot ISM component. These data were well fitted with a two-component thermal model, as it is the case for our *ASCA* data of NGC 4382. It may be interesting to do similar model comparisons for NGC 4382, but this is beyond the scope of the present paper. The spherically symmetric Pellegrini & Fabbiano (1994) models cannot be immediately adapted to an S0 galaxy.

4. CONCLUSIONS

We observed NGC 4382, one of the X-ray faint early-type galaxies, with *ASCA* SIS and GIS for $\sim$35 ks. The X-ray flux is 1.0×10^{-12} ergs s^{-1} cm^{-2} in 0.25–10 keV, consistent with the previous *ROSAT* PSPC observations. The *ASCA* data allow us to reject a low-abundance single-temperature model for this galaxy. The data is well fitted with a two-component model consisting of a very soft component ($\sim$0.3 keV) in addition to a hard stellar component ($\sim$6

keV), possibly due to the low-mass X-ray binary population of this galaxy (e.g., see bulge of M31). The acceptable range of temperatures (90% confidence) is 0.2–0.4 keV and 4–13 keV for the soft and hard components, respectively. The relative flux of the very soft component is about half the total X-ray emission in the 0.1–2 keV range and one-fourth in the 0.25–10 keV range. The data could also be fitted with more complex models. These data, while excluding a single thermal component low-abundance model, and requiring multicomponent models, cannot be used to determine the metal abundance of the soft optically thin emission. Solar values cannot be excluded.

We propose to follow up this work with careful reanalysis of the *ASCA* data of E and S0 galaxies, once these become accessible in the public domain. AXAF data will be able to disentangle the spectral properties of these galaxies from spatial variations in the ISM and therefore give us a more realistic picture.

We thank Martin Elvis for a critical reading of the manuscript, and Glen Mackie and Takaya Ohashi for useful discussions. This work was supported by NASA grant NAG5-2946 (*ASCA*), NAGW 2681 (LTSA), NASA contract NAS8-39073 (AXAF Science Center), and the KOSEF international program. This research has made use of SIMBAD, which is operated by the Centre de Donnees astronomiques de Strasbourg (CDS), France.

REFERENCES

Anders, E., & Grevesse, N. 1989, Geochim. Cosmochim. Acta, 53, 197
Avni, Y. 1976, ApJ, 210, 642
Burke, B. E., Mountain, R. W., Harrison, D. C., Bautz, M. W., Doty, J. P., Ticker, G. R., & Daniels, P. J. 1991, IEEE Trans. ED-38, 1069
Canizares, C. R., Fabbiano, G., & Trinchieri, G. 1987, ApJ, 312, 503
Day, C., Arnaud, K., Ebisawa, K., Gotthelf, E., Ingham, J., Mukai, K., & White, N. 1994, The ABC Guide to *ASCA* Data Reduction (Greenbelt: NASA GSFC *ASCA* GOF)
de Vaucouleurs, G., de Vaucouleurs, A., Corwin, H. G., Buta, R. J., Paturel, G., & Fouque, P. 1991, Third Reference Catalogue of Bright Galaxies (New York: Springer)
Dempsey, R. C., Linsky, J. L., Schmitt, J. H. M. M., & Fleming, T. A. 1993, ApJ, 413, 333
Eskridge, P. B. Fabbiano, G., & Kim, D.-W. 1995, ApJS, 97, 141
Fabbiano, G., Gioia, I. M., & Trinchieri, G. 1989, ApJ, 347, 127
Fabbiano, G., Kim, D.-W., & Trinchieri, G. 1992, ApJS, 80, 531
———. 1994, ApJ, 429, 94
Fabbiano, G., & Schweizer, F. 1995, ApJ, in press
Fabbiano, G., & Trinchieri, G. 1985, ApJ, 296, 430
Fabbiano, G., Trinchieri, G., & Van Speybroeck, L. 1987, ApJ, 316, 127
Fabian, A. C., Arnaud, K. A., Bautz, M. W., & Tawara, Y. 1994, ApJ, 436, L63
Forman, W., Jones, C., & Tucker, W. 1985, ApJ, 293, 102
Greiner, J., Hasinger, G., & Kahabka, P. 1991, A&A, 246, L17
Kahabka, P., Pietsch, W., & Hasinger, G. 1994, A&A, 288, 538
Kim, D.-W., Fabbiano, G., & Trinchieri, G. 1992a, ApJS, 80, 645
———. 1992b, ApJ, 393, 134
Matsushita, K., et al. 1994, ApJ, 436, L41
Ohashi, T., Makishima, K., Ishida, M., Tsuru, T., Tashiro, M., Mihara, T., Kohmura, Y., & Inoue, H. 1991, Proc. SPIE, 1549, 9
Pellegrini, S., & Fabbiano, G. 1994, ApJ, 429, 105
Raymond, J. C., & Smith, B. W. 1977, ApJS, 35, 419
Schmitt, J., Collura, A., Sciortino, S., Vaiana, G., Harnden, F. R., & Rosner, R. 1990, ApJ, 365, 704
Stark, A. A., Gammie, C. F., Wilson, R. W., Bally, J., Linke, R. A., Heiles, C., & Hurwitz, M. 1992, ApJS, 79, 77
Tanaka, Y., Inoue, H., & Holt, S. S. 1994, PASJ, 46, L37
Trinchieri, G., & Fabbiano, G. 1985, ApJ, 296, 447
———. 1991, ApJ, 382, 82
Trinchieri, G., Fabbiano, G., & Canizares, C. R. 1986, ApJ, 310, 637